

234 nm and 246 nm AlN-Delta-GaN quantum well deep ultraviolet light-emitting diodes

Cheng Liu,^{1,a)} Yu Kee Ooi,¹ S. M. Islam,² Huili (Grace) Xing,^{2,3,4} Debdeep Jena,^{2,3} and Jing Zhang^{1,5,b)}

¹Microsystems Engineering, Rochester Institute of Technology, Rochester, New York 14623, USA

²Department of Electrical and Computer Engineering, Cornell University, Ithaca, New York 14853, USA

³Department of Materials Science and Engineering, Cornell University, Ithaca, New York 14853, USA

⁴Kavli Institute at Cornell for Nanoscale Science, Cornell University, Ithaca, New York 14853, USA

⁵Department of Electrical and Microelectronic Engineering, Rochester Institute of Technology, Rochester, New York 14623, USA

(Received 3 October 2017; accepted 19 December 2017; published online 2 January 2018)

Deep ultraviolet (DUV) AlN-delta-GaN quantum well (QW) light-emitting diodes (LEDs) with emission wavelengths of 234 nm and 246 nm are proposed and demonstrated in this work. Our results reveal that the use of AlN-delta-GaN QW with ~ 1 – 3 monolayer GaN delta-layer can achieve a large transverse electric (TE)-polarized spontaneous emission rate instead of transverse magnetic-polarized emission, contrary to what is observed in conventional AlGaIn QW in the 230–250 nm wavelength regime. The switching of light polarization in the proposed AlN-delta-GaN QW active region is attributed to the rearrangement of the valence subbands near the Γ -point. The light radiation patterns obtained from angle-dependent electroluminescence measurements for the Molecular Beam Epitaxy (MBE)-grown 234 nm and 246 nm AlN-delta-GaN QW LEDs show that the photons are mainly emitted towards the surface rather than the edge, consistent with the simulated patterns achieved by the finite-difference time-domain modeling. The results demonstrate that the proposed AlN-delta-GaN QWs would potentially lead to high-efficiency TE-polarized surface-emitting DUV LEDs. *Published by AIP Publishing.* <https://doi.org/10.1063/1.5007835>

The development of III-nitride ultraviolet light-emitting diodes (LEDs) is of key importance for various applications such as water purification, sterilization, and high density optical recording.^{1–4} Ternary AlGaIn quantum wells (QWs) with a high Al-content have been extensively investigated as active regions for deep-ultraviolet (DUV) LEDs with wavelengths ranging from 222 nm to 350 nm.^{1–13} Nevertheless, AlGaIn QW based devices suffer from low external quantum efficiencies (η_{EQE}) [$\eta_{\text{EQE}} < 10\%$], especially for wavelengths (λ) below 250 nm.^{1–3,6–8} The main factors contributing to this limited η_{EQE} are (1) low carrier injection efficiency into the active region resulting from poor p-type doping;^{9–11} (2) low internal quantum efficiency (η_{IQE}) originating from the reduced optical matrix element and non-radiative recombination through high-density defects;^{14,15} and (3) low light extraction efficiency caused by the light absorption^{12,13} and optical polarization.¹ Specifically, transverse-electric (TE)-polarized photons with the electric field perpendicular to the c-axis ($E \perp c$) can be efficiently out-coupled from the surface of a DUV LED, contrary to the case of transverse-magnetic (TM)-polarized photons with the electric field parallel to the c-axis ($E \parallel c$).¹

To better understand the low η_{IQE} and optical polarization, the physics underlying conventional AlGaIn QW UV LEDs has been deeply explored. Studies indicate that the valence subband crossover in 3-nm conventional AlGaIn QW takes place at 68% Al-content, which leads to the severe band-mixing effect at ~ 250 nm.¹⁶ Specifically, a crystal-

field split-off (CH) subband locates at the highest energy state in the valence band for high Al-content AlGaIn QWs ($\lambda < 240$ nm) and gradually mixes with heavy-hole (HH) and light-hole (LH) subbands when pushing to the crossover point. Near the crossover point ($\lambda \sim 250$ nm), the carriers populate the three closely separated valence subbands together, leading to insufficient conduction band to HH transition (C-HH) and C-CH transition. Consequently, both TE-polarized and TM-polarized spontaneous emission rates per unit volume (R_{sp}) from AlGaIn QWs are relatively low ($< 5 \times 10^{26} \text{ s}^{-1} \text{ cm}^{-3}$) near the crossover point, as compared to TM- R_{sp} for high Al-content AlGaIn QWs. However, the carriers mainly accumulate at the CH subband for high Al-content AlGaIn QW, which results in large R_{sp} for TM-polarization and small R_{sp} for TE-polarization at shorter wavelengths (< 240 nm). In addition, TM-polarized photons at such emission wavelengths are emitted towards the edge rather than the surface, making reabsorption by defects easier than extraction, which finally results in the low η_{EQE} and “rabbit ear”-shaped light radiation pattern.¹ Therefore, nanostructures that can realize a large TE-polarized spontaneous emission rate should be explored for high-efficiency deep-UV LEDs.

Previous studies have proposed possible solutions to achieve large TE-polarized emissions in the DUV regime by using AlGaIn-delta-GaN QW¹⁷ or AlInN-delta-GaN QW.¹⁸ On the other hand, our previous work demonstrated AlN-delta-GaN QW with 3–4 monolayers (MLs) of delta-GaN emitting at 298 nm, which can be achieved with straightforward epitaxial growths.¹⁹ The main challenge at ~ 298 nm from AlGaIn QW is the quantum-confined Stark effect

^{a)}Electronic mail: cl7007@rit.edu.

^{b)}Electronic mail: Jing.Zhang@rit.edu.

(QCSE), which is addressed by the use of the AlN-delta-GaN QW as the electron and hole wavefunction overlap can be improved significantly.¹⁹ When the wavelengths are pushed to the shorter regime (<250 nm), the band mixing effect due to the existence of the valence subband crossover becomes the dominant challenge. The delta-QW design can be a promising solution to address this issue as a large separation between ground states of HH (HH1) and CH (CH1) at the Γ -point is expected.^{17,18} Furthermore, the AlN-delta-GaN QW with thinner delta-GaN layers has been grown and reported recently with shorter emission wavelengths.²⁰⁻²⁴

Therefore, in this work, we have proposed AlN-delta-GaN QW structures with 1–3 ML delta-GaN for 234 nm and 246 nm emission wavelengths to address the band mixing issue and have experimentally investigated the optical polarization and light radiation properties from these DUV LEDs. A 6-band k - p model which considers both spontaneous and piezoelectric polarization fields, the strain effect, and the carrier screening effect was employed in this study to analyze the physics of the AlN-delta-GaN QWs. Details of the simulation method and material parameters can be found in Refs. 25 and 26. In addition, a finite-difference time-domain (FDTD) method was employed to investigate the polarization-dependent light extraction properties from the investigated DUV LED structures to show the importance of polarization control. To experimentally verify the optical and polarization properties from the proposed structure, the AlN-delta-GaN QW DUV LEDs with 1–3 ML delta-GaN were grown by molecular beam epitaxy (MBE). Details of the heterostructure growth by epitaxy and the device fabrication can be found in Refs. 20–22, 27, and 28. The DUV LED devices were examined by angle-dependent and polarization-dependent electroluminescence (EL) measurements, confirming the dominant TE-polarized emission from the proposed AlN-delta-GaN QW DUV LEDs at $\lambda \sim 234$ nm and $\lambda \sim 246$ nm.

A schematic of the AlN-delta-GaN QW with the 3–4 Å delta-GaN layer is shown in the inset of Fig. 1(a). Note that the ground state electron and hole wave functions largely extend into the AlN layer, which is, together with the delta-GaN layer, forming the whole QW region. Therefore, the AlN sub-QW and AlN barrier are separately considered in the 6-band k - p calculations.¹⁹ The thicknesses of the delta-GaN layer are selected to be 3 Å and 4 Å to achieve 232 nm and 243 nm emissions, respectively, while the AlN sub-QW is designed to be 2 nm. Here, the use of the AlN-delta-GaN QW structure is aimed to address the severe valence band mixing issue at sub 250 nm so that the HH subband can be clearly separated from the CH subband to ensure dominant C-HH transition.

From the comparison in Fig. 1(a), the unpolarized spontaneous emission rates for AlN-delta-GaN QWs are significantly improved as compared to those for conventional 3-nm AlGaN QWs with similar emission wavelengths. Note that the Al-contents from the conventional QWs at sub 250 nm are very close to the AlGaN QW polarization crossover point (Al \sim 68%), which leads to small spontaneous emission rate per unit volume (R_{sp}) for both conventional structures. Specifically, the $\text{Al}_{0.67}\text{Ga}_{0.33}\text{N}$ QW with the Al composition slightly below the valence band crossover point (Al \sim 68%) suffers from a severe band mixing effect, which leads to

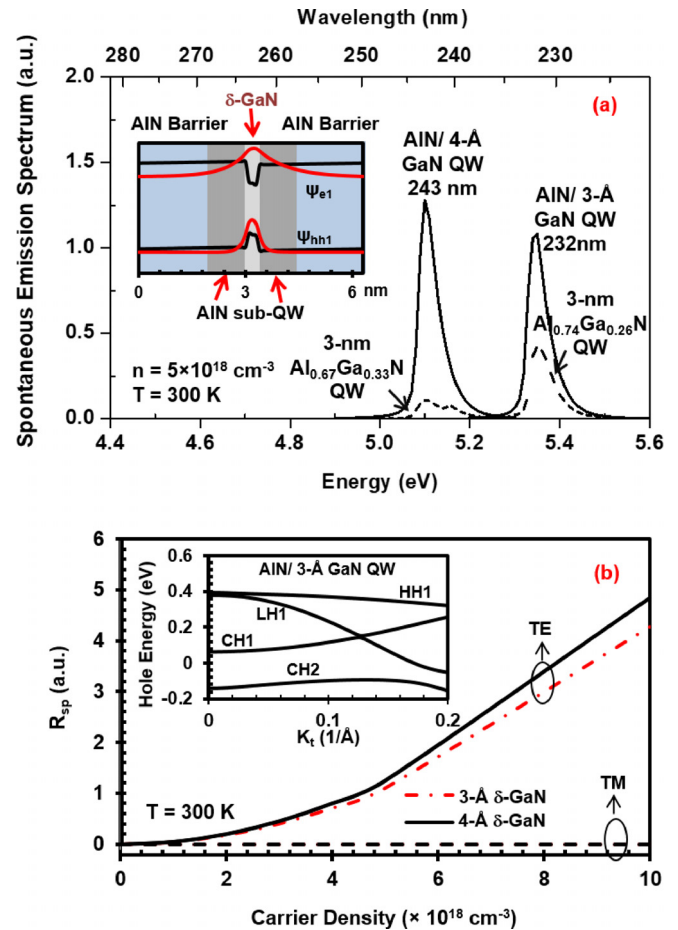


FIG. 1. (a) Spontaneous emission spectra of AlN-delta-GaN QWs and 3-nm AlGaN QWs. Inset: Energy band lineups for the AlN-delta-GaN QW with 3-Å delta-GaN and ground state electron (ψ_{e1}) and HH (ψ_{hh1}) wave functions. (b) TE-polarized (solid and dashed dotted lines) and TM-polarized (dash lines) R_{sp} as a function of carrier density for AlN-delta-GaN QWs. Inset: Valence band structures of AlN-delta-GaN QW with 3-Å delta-GaN at a carrier density of $5 \times 10^{18} \text{ cm}^{-3}$.

insufficient C-HH transition. For $\text{Al}_{0.74}\text{Ga}_{0.26}\text{N}$ QW, the CH subband occupies the highest energy level and accumulates most of the carriers, which in turn diminishes the C-HH1 transition. On the contrary, HH1 occupies the highest energy level for the proposed AlN-delta-GaN QW structure instead of the CH subband as shown in the inset of Fig. 1(b). Furthermore, the clear separation between HH1 and ground state CH subband (CH1) at the Γ point ensures dominant C-HH1 transition and large TE-polarized R_{sp} . Figure 1(b) shows the calculated TE-polarized R_{sp} and TM-polarized R_{sp} from AlN-delta-GaN QWs with different delta-GaN thicknesses as functions of carrier density (n) up to $1 \times 10^{19} \text{ cm}^{-3}$. The results show that TE-polarized R_{sp} is much larger than TM- R_{sp} for both QW structures, which is essential for high-efficiency surface-emitting deep UV LEDs.

Considering the large enhancement in TE- R_{sp} predicted by theory and the consequent potential in improving the internal quantum efficiency and the light extraction efficiency, several AlN-delta-GaN QW UV-LED devices were grown and fabricated in this study.²⁰⁻²² The schematic of the AlN-delta-GaN QW LED is shown in Fig. 2. All the devices were grown by plasma-assisted MBE on AlN/sapphire templates. To optimize the carrier injection, the polarization-induced

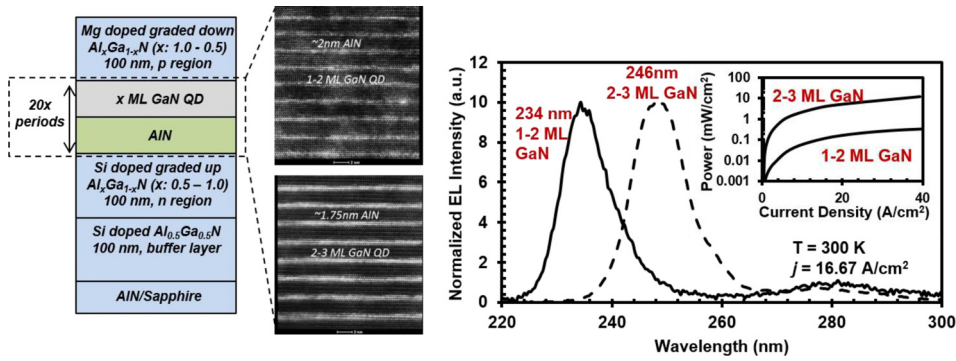


FIG. 2. Schematic of the MBE-grown AlN-delta-GaN UV LED, cross-sectional TEM images of the active regions,²¹ normalized EL spectra with $j = 16.67$ A/cm², and power as a function of current density (inset) from AlN-delta-GaN QW LEDs. The TEM images are taken from (d) and (e) of Ref. 21.

doping technique is utilized in n- and p-carrier injection layers.²¹ In order to achieve different emission wavelengths from the proposed structure, two types of AlN/GaN QWs with different delta-GaN thicknesses (1–2 MLs and 2–3 MLs, respectively) have been investigated, as evidenced by cross-sectional transmission electron microscopy (TEM) images shown in Fig. 2. After the growth, the samples were fabricated to be top-emitting LEDs with the device size of $300 \mu\text{m} \times 300 \mu\text{m}$. Room temperature electroluminescence (EL) measurements were performed on these MBE-grown AlN-delta-GaN QW LEDs at a current density (j) of 16.67 A/cm² and the measured spectra are shown in Fig. 2. A 234 nm emission peak with a full width at half maximum (FWHM) of 10.24 nm is observed from the LED device with 1–2 ML GaN delta-QW while a 246 nm emission peak with a FWHM of 11.50 nm is observed from the LED with 2–3 ML GaN delta-QW. Both structures show a small broad peak at 280 nm, which is attributed to 50% Al-content AlGaIn in the buffer layer. The emission wavelengths from the MBE-grown AlN-delta-GaN QW LEDs are consistent with that from the 6-band $k \cdot p$ simulation. The output powers of both LEDs were also measured in this study without using an integrating sphere as shown in Fig. 2. At $j = 40$ A/cm², the output power was 12 mW/cm² for the device with 2–3 ML GaN while 0.4 mW/cm² for the device with 1–2 ML GaN.

To measure the expected dominant TE-polarized emission from the designed AlN-delta-GaN QWs, the polarization properties of the emitted photons were investigated in

this study by employing polarization-dependent EL measurements with the set-up details from Ref. 19. By rotating the polarizer about the direction the light travels, two components of the emitted light, $I_{//}$ and I_{\perp} , can be resolved. Thus, the TE- and TM-polarized portion of the light can be extracted based on the $I_{//}$ and I_{\perp} at a particular angle θ , respectively.¹⁹ In this study, two angles ($\theta = 30^\circ$ and $\theta = 45^\circ$) were selected for the polarization property measurements. Figure 3 shows the polarization-dependent EL measurement results obtained from both 234 nm and 246 nm AlN-delta-GaN QW LEDs. All the results exhibit dominant TE-polarized emission. Specifically, for 234 nm LED, TE/TM ratios are measured to be 27.77 at $\theta = 30^\circ$ and 8.55 at $\theta = 45^\circ$. The corresponding degrees of polarization (P), which are defined as $P = (TE - TM)/(TE + TM)$, are extracted as ~ 0.93 and ~ 0.79 for $\theta = 30^\circ$ and $\theta = 45^\circ$, respectively, which confirms the TE-dominant emission from the device. For the case of the 246 nm device, the TE/TM ratio and P are determined as 17.731 and 0.89, respectively, at $\theta = 30^\circ$, and ~ 5.45 and 0.69, respectively, when $\theta = 45^\circ$. Therefore, the polarization-dependent EL measurements experimentally confirm that the TE-polarized emission is dominant for our proposed 234 nm and 246 nm AlN-delta-GaN QW LEDs, attributed to the topmost HH valence subband and strong C-HH transition. The agreement between the measured polarization properties and the simulation results indicates that the proposed AlN-delta-GaN QW active region has resolved the band mixing issue

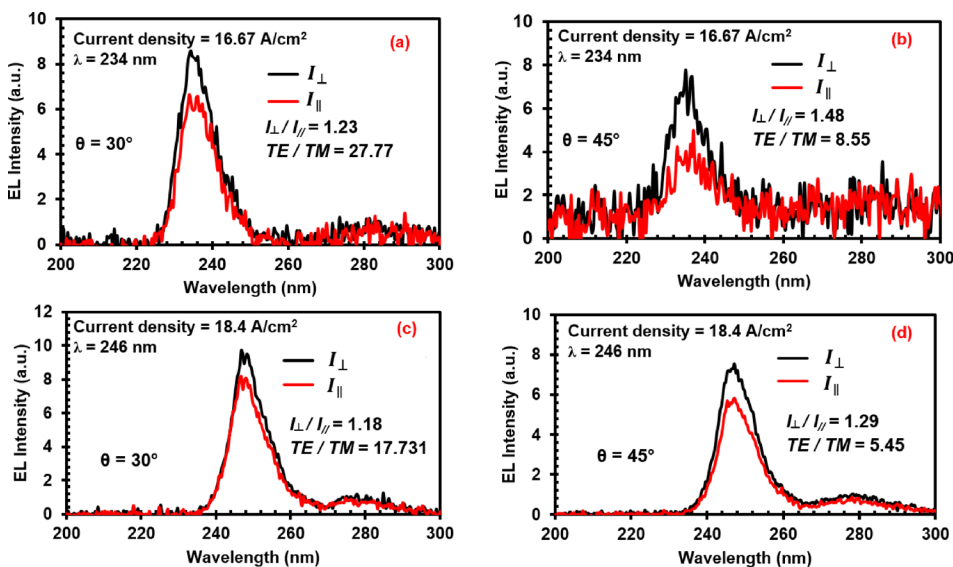


FIG. 3. Polarization-dependent EL spectra from the (a) and (b) 234 nm and (c) and (d) 246 nm AlN-delta-GaN QW UV LEDs at $\theta = 30^\circ$ and $\theta = 45^\circ$.

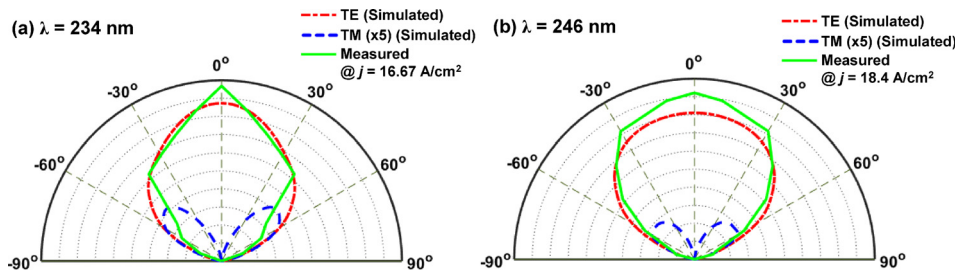


FIG. 4. FDTD simulated and measured light radiation patterns of the (a) 234 nm and (b) 246 nm AlN-delta-GaN UV LEDs.

at sub 250 nm, which can serve as a promising candidate for realizing high-efficiency TE-polarized deep-UV LEDs.

Furthermore, it is important to understand advantages of the radiation pattern due to the dominant TE-polarized emission for planar UV LEDs. The polarization-dependent light radiation patterns of the proposed delta-QW structures were investigated by both three-dimensional (3D) finite-difference time-domain (FDTD) calculations²⁹ and angle-dependent EL measurements. Details of the FDTD simulations and parameters can be found in Refs. 30–32. A single dipole source was placed at the center of the active region where TE- and TM-polarization are defined as major electric field travels in the in-plane ($E_{\perp c}$) and out-of-plane ($E_{\parallel c}$) directions, respectively. To track the light radiation pattern, a field monitor was positioned at ~ 200 nm from top of the simulated structure. As illustrated in the FDTD simulation results shown in Figs. 4(a) and 4(b), the proposed 234 nm and 246 nm LED structures exhibit significantly higher TE-polarized emissions as compared to the TM-polarized emission. In general, the radiation patterns are Lambertian-like with a large intensity observed for small angles ($<30^\circ$) for TE-polarization, while the pattern is ribbon-shaped with peak intensity at an angle of $\sim 50^\circ$ to the surface for TM-polarization. For the 234 nm LED, the TE-polarized radiation pattern has a more pointed-tip observed at 0° , indicating that the majority of the light rays are traveling at small angles from the surface of the LED. For the 246 nm LED, the intensity remains relatively strong for angles $<30^\circ$, indicating a larger escape cone for such wavelength using the proposed LED structure. In addition, the light extraction efficiency ($\eta_{\text{extraction}}$) is estimated as the ratio of the light output power measured from the top of the device to the emitted power in the active region,³⁰ and the TE- $\eta_{\text{extraction}}$ ($\sim 5\%$) is calculated as 10 times higher than the TM- $\eta_{\text{extraction}}$ ($\sim 0.5\%$).

To compare with the FDTD results, angle-dependent EL measurements were performed on the UV LEDs at a current density of 16.67 A/cm^2 for 234 nm LED and 18.4 A/cm^2 for 246 nm LED. The light radiation patterns for both devices are extracted from the measured EL spectra at different angles and plotted separately in Fig. 4. Both patterns show the highest intensity at $\theta = 0^\circ$ and the intensities drop with increasing angles, indicating that the photons mainly propagate within small angles from the top of both AlN-delta-GaN QW UV LEDs. In addition, the measured radiation patterns for the two emission wavelengths show good agreement with the simulated TE-polarized light radiation patterns, which in turn confirms the dominant TE-polarized R_{sp} from the AlN-delta-GaN QW active regions. Thus, it is expected that for the large TE-polarized R_{sp} from the delta-QW design, together with the dominant TE- $\eta_{\text{extraction}}$, those AlN-delta-

GaN QW DUV LEDs will possibly lead to enhanced extraction efficiency below 250 nm.

In conclusion, several AlN-delta-GaN QWs are proposed and demonstrated to achieve DUV emissions below 250 nm. The band structures and optical properties of the delta-QW were theoretically investigated by the 6-band $k\cdot p$ method and the results predicted that a delta-QW design could resolve the band-mixing issue and ensure a large energy separation between HH and CH subbands, resulting in sufficient C-HH1 transition and large TE- R_{sp} at 232 nm and 243 nm. The polarization properties from such QW LEDs were confirmed experimentally by the polarization-dependent EL measurements performed on MBE-grown AlN-delta-GaN QW-based LEDs with $\sim 1\text{--}2$ ML and $\sim 2\text{--}3$ ML delta-GaN layer, respectively. In addition, this study also simulated the light radiation patterns by the FDTD method, which was compared with experimental light radiation patterns to study the advantage of the dominant TE-polarized emission from planar UV LEDs. The results indicate that the light extraction efficiency for TE-polarized photons can be ~ 10 times larger than that for TM-polarized photons. Furthermore, the photons mainly propagated within small angles from the surface of the devices, which again confirmed the dominant TE-polarized emission from the proposed DUV LEDs. The theoretical prediction combined with experimental observations indicates that the use of AlN-delta-GaN QWs holds great promise for high-efficiency deep-UV LEDs.

The authors (C. Liu, Y. K. Ooi, and J. Zhang) would like to acknowledge the support by the Kate Gleason endowed professorship fund from Rochester Institute of Technology and by the Office of Naval Research under Award No. N00014-16-1-2524. The authors (S. M. Islam, H. Xing, and D. Jena) would like to thank the support from the University of Notre Dame and the NSF DMREF Program (1534303). We would also thank Dr. Sergei Rouvimov and Notre Dame Integrated Imaging Facility for technical support with the TEM images.

¹M. Kneissl and J. Rass, *III-Nitride Ultraviolet Emitters: Technology and Applications* (Springer International Publishing, 2016).

²H. Hirayama, N. Maeda, S. Fujikawa, S. Toyoda, and N. Kamata, *Jpn. J. Appl. Phys., Part 1* **53**, 100209 (2014).

³M. Kneissl, T. Kolbe, C. Chua, V. Kueller, N. Lobo, J. Stellmach, A. Knauer, H. Rodriguez, S. Einfeldt, Z. Yang, N. M. Johnson, and M. Weyers, *Semicond. Sci. Technol.* **26**, 014036 (2011).

⁴S. Vilhunen, H. Särkkä, and M. Sillanpää, *Sci. Pollut. Res.* **16**(4), 439–442 (2009).

⁵H. Hirayama, T. Yatabe, N. Noguchi, T. Ohashi, and N. Kamata, *Appl. Phys. Lett.* **91**, 071901 (2007).

⁶W. Sun, M. Shatalov, J. Deng, X. Hu, J. Yang, A. Lunev, Y. Bilenko, M. Shur, and R. Gaska, *Appl. Phys. Lett.* **96**, 061102 (2010).

- ⁷M. Shatalov, W. Sun, A. Lunev, X. Hu, A. Dobrinsky, Y. Bilenko, and J. Yang, *Appl. Phys. Express* **5**, 082101 (2012).
- ⁸T. Inazu, S. Fukahori, C. Pernot, M. H. Kim, T. Fujita, Y. Nagasawa, A. Hirano, M. Ippommatsu, M. Iwaya, T. Takeuchi, S. Kamiyama, M. Yamaguchi, Y. Honda, H. Amano, and I. Akasaki, *Jpn. J. Appl. Phys.* **50**, 122101 (2011).
- ⁹F. Mehnke, C. Kuhn, M. Guttman, C. Reich, T. Kolbe, V. Kueller, A. Knauer, M. Lapeyrade, S. Einfeldt, J. Rass, T. Wernicke, M. Weyers, and M. Kneissl, *Appl. Phys. Lett.* **105**, 051113 (2014).
- ¹⁰T. Kolbe, F. Mehnke, M. Guttman, C. Kuhn, J. Rass, T. Wernicke, and M. Kneissl, *Appl. Phys. Lett.* **103**, 031109 (2013).
- ¹¹Y. Zhang, S. Krishnamoorthy, J. M. Johnson, F. Akyol, A. Allerman, M. W. Moseley, A. Armstrong, J. Hwang, and S. Rajan, *Appl. Phys. Lett.* **106**, 141103 (2015).
- ¹²M. Jo, N. Maeda, and H. Hirayama, *Appl. Phys. Express* **9**, 012102 (2016).
- ¹³Y. Zhang, A. A. Allerman, S. Krishnamoorthy, F. Akyol, M. W. Moseley, A. M. Armstrong, and S. Rajan, *Appl. Phys. Express* **9**, 052102 (2016).
- ¹⁴S. F. Chichibu, A. Uedono, T. Onuma, B. A. Haskell, A. Chakraborty, T. Koyama, P. T. Fini, S. Keller, S. P. DenBaars, J. S. Speck, U. K. Mishra, S. Nakamura, S. Yamaguchi, S. Kamiyama, H. Amano, I. Akasaki, J. Han, and T. Sota, *Nat. Mater.* **5**, 810–816 (2006).
- ¹⁵S. Karpov and Y. N. Makarov, *Appl. Phys. Lett.* **81**, 4721 (2002).
- ¹⁶J. Zhang, H. Zhao, and N. Tansu, *Appl. Phys. Lett.* **97**, 111105 (2010).
- ¹⁷J. Zhang, H. Zhao, and N. Tansu, *Appl. Phys. Lett.* **98**, 171111 (2011).
- ¹⁸C. Liu, Y. K. Ooi, and J. Zhang, *J. Appl. Phys.* **119**, 083102 (2016).
- ¹⁹C. Liu, Y. K. Ooi, S. M. Islam, J. Verma, H. Xing, D. Jena, and J. Zhang, *Appl. Phys. Lett.* **110**, 071103 (2017).
- ²⁰S. M. Islam, V. Protasenko, S. Rouvimov, H. Xing, and D. Jena, *Jpn. J. Appl. Phys., Part 1* **55**, 05FF06 (2016).
- ²¹S. M. Islam, K. Lee, V. Protasenko, S. Rouvimov, S. Bharadwaj, H. Xing, and D. Jena, *Appl. Phys. Lett.* **110**, 041108 (2017).
- ²²D. Bayerl, S. M. Islam, C. M. Jones, V. Protasenko, D. Jena, and E. Kioupakis, *Appl. Phys. Lett.* **109**, 241102 (2016).
- ²³S. M. Islam, V. Protasenko, K. Lee, S. Rouvimov, J. Verma, H. Xing, and D. Jena, *Appl. Phys. Lett.* **111**, 091104 (2017).
- ²⁴Y. Taniyasu and M. Kasu, *Appl. Phys. Lett.* **99**, 251112 (2011).
- ²⁵S. L. Chuang, *Physics of Photonic Devices*, 2nd ed. (Wiley, New York, 2009), Chap. IV.
- ²⁶H. Zhao, R. A. Arif, Y. K. Ee, and N. Tansu, *IEEE J. Quantum Electron.* **45**, 66 (2009).
- ²⁷J. Verma, S. M. Islam, V. Protasenko, P. K. Kandaswamy, H. Xing, and D. Jena, *Appl. Phys. Lett.* **104**, 021105 (2014).
- ²⁸J. Verma, P. Kandaswamy, V. Protasenko, A. Verma, H. Xing, and D. Jena, *Appl. Phys. Lett.* **102**, 041103 (2013).
- ²⁹FullWAVE, Synopsys's Optical Solutions Group, <https://optics.synopsys.com> for information about FDTD simulation using Synopsys's RSoft FullWave.
- ³⁰Y. K. Ooi, C. Liu, and J. Zhang, *IEEE Photonics J.* **9**, 4501712 (2017).
- ³¹E. D. Palik, *Handbook of Optical Constants of Solids* (Academic Press, 1998).
- ³²C. H. Yan, H. Yao, J. M. Van Hove, M. Wowchak, P. P. Chow, and J. M. Zavada, *J. Appl. Phys.* **88**, 3463 (2000).